

K. Kaufman⁵¹, K. Kawabe¹⁷, S. Kawamura¹², F. Kawazoe^{9,10}, D. Keitel^{9,10}, D. Kelley²², W. Kells¹, D. G. Keppel¹,
 Z. Keresztes⁷⁰, A. Khalaidovski^{9,10}, F. Y. Khalili³⁰, E. A. Khazanov⁷⁹, B. K. Kim⁷⁷, C. Kim⁸⁰, H. Kim^{9,10},
 K. Kim⁸¹, N. Kim²⁶, Y. M. Kim⁵³, P. J. King¹, D. L. Kinzel⁶, J. S. Kissel²³, S. Klimenko¹⁵, J. Kline¹³,
 K. Kokeyama⁴⁸, V. Kondrashov¹, S. Koranda¹³, W. Z. Korth¹, I. Kowalska^{27b}, D. Kozak¹, V. Kringel^{9,10},
 B. Krishnan¹⁹, A. Królak^{27a,27e}, G. Kuehn^{9,10}, P. Kumar²², R. Kumar³, R. Kurdyumov²⁶, P. Kwee²³, P. K. Lam⁵⁴,
 M. Landry¹⁷, A. Langley⁶⁵, B. Lantz²⁶, N. Lastzka^{9,10}, C. Lawrie³, A. Lazzarini¹, A. Le Roux⁶, P. Leaci¹⁹,
 C. H. Lee⁵³, H. K. Lee⁸¹, H. M. Lee⁸², J. R. Leong^{9,10}, I. Leonor⁴⁰, N. Leroy^{31a}, N. Letendre⁴, V. Lhuillier¹⁷,
 J. Li⁴⁶, T. G. F. Li^{11a}, P. E. Lindquist¹, V. Litvine¹, Y. Liu⁴⁶, Z. Liu¹⁵, N. A. Lockerbie⁸³, D. Lodhia¹⁸,
 J. Logue³, M. Lorenzini^{39a}, V. Lorette^{31b}, M. Lormand⁶, G. Losurdo^{39a}, J. Lough²², M. Lubinski¹⁷, H. Lück^{9,10},
 A. P. Lundgren^{9,10}, J. Macarthur³, E. Macdonald³, B. Machenschalk^{9,10}, M. MacInnis²³, D. M. Macleod⁷,
 M. Mageswaran¹, K. Mailand¹, E. Majorana^{16a}, I. Maksimovic^{31b}, V. Malvezzi^{57a}, N. Man^{35a}, I. Mandel¹⁸,
 V. Mandic⁶³, M. Mantovani^{14a}, F. Marchesoni^{38ac}, F. Marion⁴, S. Márka²⁵, Z. Márka²⁵, A. Markosyan²⁶, E. Maros¹,
 J. Marque²¹, F. Martelli^{39a,39b}, I. W. Martin³, R. M. Martin¹⁵, J. N. Marx¹, K. Mason²³, A. Masserot⁴,
 F. Matichard²³, L. Matone²⁵, R. A. Matzner⁸⁴, N. Mavalvala²³, G. Mazzolo^{9,10}, R. McCarthy¹⁷, D. E. McClelland⁵⁴,
 S. C. McGuire⁸⁵, G. McIntyre¹, J. McIver⁴⁴, G. D. Meadors⁴⁷, M. Mehmet^{9,10}, T. Meier^{10,9}, A. Melatos⁵⁶,
 A. C. Melissinos⁸⁶, G. Mendell¹⁷, D. F. Menéndez³⁴, R. A. Mercer¹³, S. Meshkov¹, C. Messenger⁷, M. S. Meyer⁶,
 H. Miao⁵¹, C. Michel³⁶, L. Milano^{5a,5b}, J. Miller⁵⁴, Y. Minenkov^{57a}, C. M. F. Mingarelli¹⁸, V. P. Mitrofanov³⁰,
 G. Mitselmakher¹⁵, R. Mittleman²³, B. Moe¹³, M. Mohan²¹, S. R. P. Mohapatra⁴⁴, D. Moraru¹⁷, G. Moreno¹⁷,
 N. Morgado³⁶, A. Morgia^{57a,57b}, T. Mori¹², S. R. Morriss²⁸, S. Mosca^{5a,5b}, K. Mossavi^{9,10}, B. Mours⁴,
 C. M. Mow-Lowry⁵⁴, C. L. Mueller¹⁵, G. Mueller¹⁵, S. Mukherjee²⁸, A. Mullavey^{48,54}, H. Müller-Ebhardt^{9,10},
 J. Munch⁸⁷, D. Murphy²⁵, P. G. Murray³, A. Mytidis¹⁵, T. Nash¹, L. Naticchioni^{16a,16b}, V. Necula¹⁵, J. Nelson³,
 I. Neri^{38a,38b}, G. Newton³, T. Nguyen⁵⁴, A. Nishizawa¹², A. Nitz²², F. Nocera²¹, D. Nolting⁶, M. E. Normandin²⁸,
 L. Nuttall⁷, E. Ochsner¹³, J. O'Dell⁷¹, E. Oelker²³, G. H. Ogin¹, J. J. Oh⁸⁸, S. H. Oh⁸⁸, R. G. Oldenberg¹³,
 B. O'Reilly⁶, R. O'Shaughnessy¹³, C. Osthelder¹, C. D. Ott⁵¹, D. J. Ottaway⁸⁷, R. S. Ottens¹⁵, H. Overmier⁶,
 B. J. Owen³⁴, A. Page¹⁸, L. Palladino^{57a,57c}, C. Palomba^{16a}, Y. Pan⁴², C. Pankow¹³, F. Paoletti^{14a,21},
 R. Paoletti^{14ac}, M. A. Papa^{19,13}, M. Parisi^{5a,5b}, A. Pasqualetti²¹, R. Passaquieti^{14a,14b}, D. Passuello^{14a}, M. Pedraza¹,
 S. Penn⁷⁸, A. Perreca²², G. Persichetti^{5a,5b}, M. Phelps¹, M. Pichot^{35a}, M. Pickenpack^{9,10}, F. Piergiovanni^{39a,39b},
 V. Pierro⁸, M. Pihlaja⁶³, L. Pinar³⁶, I. M. Pinto⁸, M. Pitkin³, H. J. Pletsch^{9,10}, M. V. Plissi³, R. Poggiani^{14a,14b},
 J. Pöld^{9,10}, F. Postiglione⁵⁸, C. Poux¹, M. Prato⁵², V. Predoi⁷, T. Prestegard⁶³, L. R. Price¹, M. Prijatelj^{9,10},
 M. Principe⁸, S. Privitera¹, R. Prix^{9,10}, G. A. Prodi^{64a,64b}, L. G. Prokhorov³⁰, O. Puncken^{9,10}, M. Punturo^{38a},
 P. Puppo^{16a}, V. Quetschke²⁸, R. Quitzow-James⁴⁰, F. J. Raab¹⁷, D. S. Rabeling^{11a,11b}, I. Rácz⁶¹, H. Radkins¹⁷,
 P. Raffai^{25,68}, M. Rakhmanov²⁸, C. Ramet⁶, B. Rankins⁴⁹, P. Rapagnani^{16a,16b}, V. Raymond⁶⁶, V. Re^{57a,57b},
 C. M. Reed¹⁷, T. Reed⁸⁹, T. Regimbau^{35a}, S. Reid³, D. H. Reitze¹, F. Ricci^{16a,16b}, R. Riesen⁶, K. Riles⁴⁷,
 M. Roberts²⁶, N. A. Robertson^{1,3}, F. Robinet^{31a}, C. Robinson⁷, E. L. Robinson¹⁹, A. Rocchi^{57a}, S. Roddy⁶,
 C. Rodriguez⁶⁶, M. Rodruck¹⁷, L. Rolland⁴, J. G. Rollins¹, R. Romano^{5a,5c}, J. H. Romie⁶, D. Rosińska^{27c,27f},
 C. Röver^{9,10}, S. Rowan³, A. Rüdiger^{9,10}, P. Ruggi²¹, K. Ryan¹⁷, F. Salemi^{9,10}, L. Sammut⁵⁶, V. Sandberg¹⁷,
 S. Sankar²³, V. Sannibale¹, L. Santamaría¹, I. Santiago-Prieto³, G. Santostasi⁹⁰, E. Saracco³⁶, B. Sassolas³⁶,
 B. S. Sathyaprakash⁷, P. R. Saulson²², R. L. Savage¹⁷, R. Schilling^{9,10}, R. Schnabel^{9,10}, R. M. S. Schofield⁴⁰,
 B. Schulz^{9,10}, B. F. Schutz^{19,7}, P. Schwinberg¹⁷, J. Scott³, S. M. Scott⁵⁴, F. Seifert¹, D. Sellers⁶, D. Sentenac²¹,
 A. Sergeev⁷⁹, D. A. Shaddock⁵⁴, M. Shaltev^{9,10}, B. Shapiro²³, P. Shawhan⁴², D. H. Shoemaker²³, T. L. Sidery¹⁸,
 X. Siemens¹³, D. Sigg¹⁷, D. Simakov^{9,10}, A. Singer¹, L. Singer¹, A. M. Sintes⁴³, G. R. Skelton¹³,
 B. J. J. Slagmolen⁵⁴, J. Slutsky⁴⁸, J. R. Smith², M. R. Smith¹, R. J. E. Smith¹⁸, N. D. Smith-Lefebvre²³,
 K. Somiya⁵¹, B. Sorazu³, F. C. Speirits³, L. Sperandio^{57a,57b}, M. Stefszky⁵⁴, E. Steinert¹⁷, J. Steinlechner^{9,10},
 S. Steinlechner^{9,10}, S. Steplewski³⁷, A. Stochino¹, R. Stone²⁸, K. A. Strain³, S. E. Strigin³⁰, A. S. Stroerer²⁸,
 R. Sturani^{39a,39b}, A. L. Stuver⁶, T. Z. Summerscales⁹¹, M. Sung⁴⁸, S. Susmithan³³, P. J. Sutton⁷, B. Swinkels²¹,
 G. Szeifert⁶⁸, M. Tacca²¹, L. Taffarelo^{64c}, D. Talukder³⁷, D. B. Tanner¹⁵, S. P. Tarabrin^{9,10}, R. Taylor¹,
 A. P. M. ter Braack^{11a}, P. Thomas¹⁷, K. A. Thorne⁶, K. S. Thorne⁵¹, E. Thrane⁶³, A. Thüring^{10,9}, C. Tittler³⁴,
 K. V. Tokmakov⁸³, C. Tomlinson⁶⁰, A. Toncelli^{14a,14b}, M. Tonelli^{14a,14b}, O. Torre^{14a,14c}, C. V. Torres²⁸,
 C. I. Torrie^{1,3}, E. Tournefier⁴, F. Travasso^{38a,38b}, G. Traylor⁶, M. Tse²⁵, D. Ugolini⁹², H. Vahlbruch^{10,9},
 G. Vajente^{14a,14b}, J. F. J. van den Brand^{11a,11b}, C. Van Den Broeck^{11a}, S. van der Putten^{11a}, A. A. van Veggel³,
 S. Vass¹, M. Vasuth⁶¹, R. Vaulin²³, M. Vavoulidis^{31a}, A. Vecchio¹⁸, G. Vedovato^{64c}, J. Veitch⁷, P. J. Veitch⁸⁷,
 K. Venkateswara⁹³, D. Verkindt⁴, F. Vetrano^{39a,39b}, A. Viceré^{39a,39b}, A. E. Villar¹, J.-Y. Vinet^{35a}, S. Vitale^{11a},
 H. Vocca^{38a}, C. Vorvick¹⁷, S. P. Vyatchanin³⁰, A. Wade⁵⁴, L. Wade¹³, M. Wade¹³, S. J. Waldman²³, L. Wallace¹,

Y. Wan⁴⁶, M. Wang¹⁸, X. Wang⁴⁶, A. Wanner^{9,10}, R. L. Ward²⁴, M. Was^{31a}, M. Weinert^{9,10}, A. J. Weinstein¹, R. Weiss²³, T. Welborn⁶, L. Wen^{51,33}, P. Wessels^{9,10}, M. West²², T. Westphal^{9,10}, K. Wette^{9,10}, J. T. Whelan⁶⁷, S. E. Whitcomb^{1,33}, D. J. White⁶⁰, B. F. Whiting¹⁵, K. Wiesner^{9,10}, C. Wilkinson¹⁷, P. A. Willems¹, L. Williams¹⁵, R. Williams¹, B. Willke^{9,10}, M. Wimmer^{9,10}, L. Winkelmann^{9,10}, W. Winkler^{9,10}, C. C. Wipf²³, A. G. Wiseman¹³, H. Wittel^{9,10}, G. Woan³, R. Wooley⁶, J. Worden¹⁷, J. Yablon⁶⁶, I. Yakushin⁶, H. Yamamoto¹, K. Yamamoto^{64b,64d}, C. C. Yancey⁴², H. Yang⁵¹, D. Yeaton-Massey¹, S. Yoshida⁹⁴, M. Yvert⁴, A. Zadrożny^{27e}, M. Zanolin⁷², J.-P. Zendri^{64c}, F. Zhang⁴⁶, L. Zhang¹, C. Zhao³³, N. Zotov⁸⁹, M. E. Zucker²³, and J. Zweigig¹

¹LIGO - California Institute of Technology, Pasadena, CA 91125, USA

²California State University Fullerton, Fullerton CA 92831 USA

³SUPA, University of Glasgow, Glasgow, G12 8QQ, United Kingdom

⁴Laboratoire d'Annecy-le-Vieux de Physique des Particules (LAPP),
Université de Savoie, CNRS/IN2P3, F-74941 Annecy-Le-Vieux, France

⁵INFN, Sezione di Napoli ^a; Università di Napoli 'Federico II' ^b, Complesso Universitario di Monte S. Angelo,
I-80126 Napoli; Università di Salerno, Fisciano, I-84084 Salerno ^c, Italy

⁶LIGO - Livingston Observatory, Livingston, LA 70754, USA

⁷Cardiff University, Cardiff, CF24 3AA, United Kingdom

⁸University of Sannio at Benevento, I-82100 Benevento, Italy and INFN (Sezione di Napoli), Italy

⁹Albert-Einstein-Institut, Max-Planck-Institut für Gravitationsphysik, D-30167 Hannover, Germany

¹⁰Leibniz Universität Hannover, D-30167 Hannover, Germany

¹¹Nikhef, Science Park, Amsterdam, The Netherlands ^a; VU University Amsterdam,
De Boelelaan 1081, 1081 HV Amsterdam, The Netherlands ^b

¹²National Astronomical Observatory of Japan, Tokyo 181-8588, Japan

¹³University of Wisconsin-Milwaukee, Milwaukee, WI 53201, USA

¹⁴INFN, Sezione di Pisa ^a; Università di Pisa ^b; I-56127 Pisa; Università di Siena, I-53100 Siena ^c, Italy

¹⁵University of Florida, Gainesville, FL 32611, USA

¹⁶INFN, Sezione di Roma ^a; Università 'La Sapienza' ^b, I-00185 Roma, Italy

¹⁷LIGO - Hanford Observatory, Richland, WA 99352, USA

¹⁸University of Birmingham, Birmingham, B15 2TT, United Kingdom

¹⁹Albert-Einstein-Institut, Max-Planck-Institut für Gravitationsphysik, D-14476 Golm, Germany

²⁰Montana State University, Bozeman, MT 59717, USA

²¹European Gravitational Observatory (EGO), I-56021 Cascina (PI), Italy

²²Syracuse University, Syracuse, NY 13244, USA

²³LIGO - Massachusetts Institute of Technology, Cambridge, MA 02139, USA

²⁴APC, AstroParticule et Cosmologie, Université Paris Diderot,
CNRS/IN2P3, CEA/Irfu, Observatoire de Paris, Sorbonne Paris Cité,
10, rue Alice Domon et Léonie Duquet, 75205 Paris Cedex 13, France

²⁵Columbia University, New York, NY 10027, USA

²⁶Stanford University, Stanford, CA 94305, USA

²⁷IM-PAN 00-956 Warsaw ^a; Astronomical Observatory Warsaw University 00-478 Warsaw ^b; CAMK-PAN 00-716 Warsaw ^c;
Białystok University 15-424 Białystok ^d; NCBJ 05-400 Świerk-Otwock ^e; Institute of Astronomy 65-265 Zielona Góra ^f, Poland

²⁸The University of Texas at Brownsville, Brownsville, TX 78520, USA

²⁹San Jose State University, San Jose, CA 95192, USA

³⁰Moscow State University, Moscow, 119992, Russia

³¹LAL, Université Paris-Sud, IN2P3/CNRS, F-91898 Orsay ^a; ESPCI, CNRS, F-75005 Paris ^b, France

³²NASA/Goddard Space Flight Center, Greenbelt, MD 20771, USA

³³University of Western Australia, Crawley, WA 6009, Australia

³⁴The Pennsylvania State University, University Park, PA 16802, USA

³⁵Université Nice-Sophia-Antipolis, CNRS, Observatoire de la Côte d'Azur,
F-06304 Nice ^a; Institut de Physique de Rennes, CNRS, Université de Rennes 1, 35042 Rennes ^b, France

³⁶Laboratoire des Matériaux Avancés (LMA), IN2P3/CNRS, F-69622 Villeurbanne, Lyon, France

³⁷Washington State University, Pullman, WA 99164, USA

³⁸INFN, Sezione di Perugia ^a; Università di Perugia ^b,

I-06123 Perugia; Università di Camerino, Dipartimento di Fisica ^c, I-62032 Camerino, Italy

³⁹INFN, Sezione di Firenze, I-50019 Sesto Fiorentino ^a; Università degli Studi di Urbino 'Carlo Bo', I-61029 Urbino ^b, Italy

⁴⁰University of Oregon, Eugene, OR 97403, USA

⁴¹Laboratoire Kastler Brossel, ENS, CNRS, UPMC,
Université Pierre et Marie Curie, 4 Place Jussieu, F-75005 Paris, France

⁴²University of Maryland, College Park, MD 20742 USA

⁴³Universitat de les Illes Balears, E-07122 Palma de Mallorca, Spain

⁴⁴University of Massachusetts - Amherst, Amherst, MA 01003, USA

⁴⁵Canadian Institute for Theoretical Astrophysics,
University of Toronto, Toronto, Ontario, M5S 3H8, Canada

- ⁴⁶*Tsinghua University, Beijing 100084 China*
- ⁴⁷*University of Michigan, Ann Arbor, MI 48109, USA*
- ⁴⁸*Louisiana State University, Baton Rouge, LA 70803, USA*
- ⁴⁹*The University of Mississippi, University, MS 38677, USA*
- ⁵⁰*Charles Sturt University, Wagga Wagga, NSW 2678, Australia*
- ⁵¹*Caltech-CaRT, Pasadena, CA 91125, USA*
- ⁵²*INFN, Sezione di Genova; I-16146 Genova, Italy*
- ⁵³*Pusan National University, Busan 609-735, Korea*
- ⁵⁴*Australian National University, Canberra, ACT 0200, Australia*
- ⁵⁵*Carleton College, Northfield, MN 55057, USA*
- ⁵⁶*The University of Melbourne, Parkville, VIC 3010, Australia*
- ⁵⁷*INFN, Sezione di Roma Tor Vergata^a; Università di Roma Tor Vergata, I-00133 Roma^b; Università dell'Aquila, I-67100 L'Aquila^c, Italy*
- ⁵⁸*University of Salerno, I-84084 Fisciano (Salerno), Italy*
- ⁵⁹*Instituto Nacional de Pesquisas Espaciais, 12227-010 - São José dos Campos, SP, Brazil*
- ⁶⁰*The University of Sheffield, Sheffield S10 2TN, United Kingdom*
- ⁶¹*Wigner RCP, RMKI, H-1121 Budapest, Konkoly Thege Miklós út 29-33, Hungary*
- ⁶²*Inter-University Centre for Astronomy and Astrophysics, Pune - 411007, India*
- ⁶³*University of Minnesota, Minneapolis, MN 55455, USA*
- ⁶⁴*INFN, Gruppo Collegato di Trento^a and Università di Trento^b, I-38050 Povo, Trento, Italy; INFN, Sezione di Padova^c and Università di Padova^d, I-35131 Padova, Italy*
- ⁶⁵*California Institute of Technology, Pasadena, CA 91125, USA*
- ⁶⁶*Northwestern University, Evanston, IL 60208, USA*
- ⁶⁷*Rochester Institute of Technology, Rochester, NY 14623, USA*
- ⁶⁸*Eötvös Loránd University, Budapest, 1117 Hungary*
- ⁶⁹*University of Cambridge, Cambridge, CB2 1TN, United Kingdom*
- ⁷⁰*University of Szeged, 6720 Szeged, Dóm tér 9, Hungary*
- ⁷¹*Rutherford Appleton Laboratory, HSIC, Chilton, Didcot, Oxon OX11 0QX United Kingdom*
- ⁷²*Embry-Riddle Aeronautical University, Prescott, AZ 86301 USA*
- ⁷³*Perimeter Institute for Theoretical Physics, Ontario, N2L 2Y5, Canada*
- ⁷⁴*American University, Washington, DC 20016, USA*
- ⁷⁵*University of New Hampshire, Durham, NH 03824, USA*
- ⁷⁶*University of Southampton, Southampton, SO17 1BJ, United Kingdom*
- ⁷⁷*Korea Institute of Science and Technology Information, Daejeon 305-806, Korea*
- ⁷⁸*Hobart and William Smith Colleges, Geneva, NY 14456, USA*
- ⁷⁹*Institute of Applied Physics, Nizhny Novgorod, 603950, Russia*
- ⁸⁰*Lund Observatory, Box 43, SE-221 00, Lund, Sweden*
- ⁸¹*Hanyang University, Seoul 133-791, Korea*
- ⁸²*Seoul National University, Seoul 151-742, Korea*
- ⁸³*University of Strathclyde, Glasgow, G1 1XQ, United Kingdom*
- ⁸⁴*The University of Texas at Austin, Austin, TX 78712, USA*
- ⁸⁵*Southern University and A&M College, Baton Rouge, LA 70813, USA*
- ⁸⁶*University of Rochester, Rochester, NY 14627, USA*
- ⁸⁷*University of Adelaide, Adelaide, SA 5005, Australia*
- ⁸⁸*National Institute for Mathematical Sciences, Daejeon 305-390, Korea*
- ⁸⁹*Louisiana Tech University, Ruston, LA 71272, USA*
- ⁹⁰*McNeese State University, Lake Charles, LA 70609 USA*
- ⁹¹*Andrews University, Berrien Springs, MI 49104 USA*
- ⁹²*Trinity University, San Antonio, TX 78212, USA*
- ⁹³*University of Washington, Seattle, WA, 98195-4290, USA*
- ⁹⁴*Southeastern Louisiana University, Hammond, LA 70402, USA*

We report a search for gravitational waves from the inspiral, merger and ringdown of binary black holes (BBH) with total mass between 25 and 100 solar masses, in data taken at the LIGO and Virgo observatories between July 7, 2009 and October 20, 2010. The maximum sensitive distance of the detectors over this period for a $(20,20)M_{\odot}$ coalescence was 300 Mpc. No gravitational wave signals were found. We thus report upper limits on the astrophysical coalescence rates of BBH as a function of the component masses for non-spinning components, and also evaluate the dependence of the search sensitivity on component spins aligned with the orbital angular momentum. We find an upper limit at 90% confidence on the coalescence rate of BBH with non-spinning components of mass between 19 and $28 M_{\odot}$ of 3.3×10^{-7} mergers $\text{Mpc}^{-3}\text{yr}^{-1}$.

I. OVERVIEW

Binary black hole (BBH) systems are a major class of possible gravitational-wave (GW) sources accessible to ground-based interferometric detectors such as LIGO [1] and Virgo [2]. As described in [3], for higher-mass BBH systems, the merger and ringdown stages of the coalescence come into the detectors' sensitive frequency range and the search sensitivity is improved by using inspiral-merger-ringdown (IMR) matched filter templates. Such templates were used in [3] to search for compact binary coalescences (CBCs) signals with total masses between 25 and $100 M_{\odot}$ in LIGO data.

Our knowledge of possible high-mass BBH source systems [4] is based on a combination of observations and astrophysical modelling: a summary of the recent evidence on both fronts is provided in [3]. A number of indicators point to the possibility of forming binary black holes with component masses m_1, m_2 of $\sim 20 - 30 M_{\odot}$ and beyond: in particular, predictions of the future fate of the high-mass Wolf-Rayet X-ray binaries IC10 X-1 and NGC 300 X-1 [5]; analyses of dynamical BBH formation in dense stellar environments; the growing evidence for the existence of intermediate-mass black holes (e.g. [6]); and population-synthesis modeling of low-metallicity environments [7]. A recent population-synthesis study [8] that considered a wide range of astrophysical models found that in low-metallicity environments or under the assumption of weak wind-driven mass loss rates, the distribution of BBH chirp masses $\mathcal{M} \equiv (m_1 m_2)^{3/5} (m_1 + m_2)^{-1/5}$ extended above $30 M_{\odot}$; for comparison, the chirp mass of a binary with component masses $(50, 50) M_{\odot}$ is $43.5 M_{\odot}$.

In this paper we report a search for GW signals from coalescence of binary black holes with non-spinning components having masses m_1, m_2 between 1 and $99 M_{\odot}$ and total mass $M \equiv m_1 + m_2$ between 25 and $100 M_{\odot}$, over the most recently taken coincident data from the LIGO and Virgo observatories. A companion paper [9] describes a search for low-mass binary inspiral signals with $2 \leq M/M_{\odot} \leq 25$ over these data, while a search of previous LIGO and Virgo data for BBH mergers signals with total mass $100-450 M_{\odot}$ is reported in [10].

The joint science run used in this work—LIGO's sixth science run (S6) and Virgo's second (VSR2) and third (VSR3) science runs—was the most sensitive to date to signals from coalescing BBH; this search was also the first for high-mass BBH coalescences in Virgo data. We describe the detectors and the joint S6-VSR2/VSR3 science run in Section II. The search pipeline used here is similar to that of [3, 11], with changes to the ranking of events to account for variability of the noise background over the parameter space of the search and between detectors. We give a brief overview of the pipeline and describe changes relative to previous searches in Section III.

The output of the analysis is a set of *coincident events* where a potentially significant signal was seen in two or more detectors with consistent coalescence times and

mass parameters. Events occurring at times when the detectors' environmental or instrumental monitor channels indicated a problem likely to corrupt the data are *vetoed*: either removed from the search or placed in a separate category, depending on the severity of the problem. The significance of each remaining candidate event is measured by its false alarm rate (FAR), the expected rate of noise events with a detection statistic value (defined in Section III) at least as large as the candidate's.

As in previous LIGO-Virgo searches, the distribution of noise events in non-Gaussian data is estimated by applying unphysical time-shifts to data from different detectors. Events with low estimated FAR are subject to a detailed followup procedure to check the consistency of the detector outputs around the event time and determine whether environmental disturbances or detector malfunction could have caused a spurious signal at that time. The search did not find any significant gravitational-wave candidate events; we describe the most significant events in Section IV.

We then evaluated the sensitivity of the search to coalescing BBH at astrophysical distances by analyzing a large number of simulated signals (“injections”) added to the detector data. These are used to estimate the sensitivity of the search in terms of the sensitive distance in Mpc within which we would be able to detect a signal, averaged over the observation time and over source sky location and orientation, with significance above that of the loudest event observed in the search. From this we set upper limits on the rate of such coalescences as a function of their component masses. For this purpose we used two recently-developed families of IMR waveforms. The improved EOBNRv2 family [12] was used to assess the sensitive range of the search for comparison with the previous high-mass BBH search and to set upper limits on astrophysical coalescence rates; the IMRPhenomB waveform family [13] was used to assess the sensitivity of the search to coalescences of BBH with spinning components, where the component spins are aligned with the orbital angular momentum and thus the system does not precess. We describe the injections performed and the resulting sensitivity distances and upper limits in Section V.

To conclude, we briefly discuss outstanding issues for high-mass BBH searches and prospects for the advanced detector era in Section VI.

II. S6 AND VSR2/VSR3 OBSERVATIONS

The US-based Laser Interferometer Gravitational-wave Observatory (LIGO) comprises two sites: Hanford, WA and Livingston, LA. The data used in this search were taken during LIGO's sixth science run (S6), which took place between July 7, 2009 and October 20, 2010. During S6 each of these sites operated a single 4-km laser interferometer, denoted as H1 and L1 respectively. The 2-km H2 instrument at the Hanford site which operated

in earlier science runs was not operational in S6. Following LIGO’s fifth science run (S5) [1], several hardware changes were made to the LIGO detectors in order to install and test prototypes of Advanced LIGO [14] technology. These changes included the installation of higher-powered lasers, and the implementation of a DC readout system that included a new output mode cleaner on an Advanced LIGO seismic isolation table [15]. In addition, the hydraulic seismic isolation systems were improved by fine-tuning their feed-forward paths.

The Virgo detector (denoted V1) is a single, 3-km laser interferometer located in Cascina, Italy. The data used in this search were taken from both Virgo’s second science run (VSR2) [16], which ran from July 7, 2009 to January 11, 2010, and third science run (VSR3), which ran from August 11, 2010 to October 20, 2010. In the period between the first Virgo science run (VSR1) and VSR2, several enhancements were made to the Virgo detector: a more powerful laser and a thermal compensation system were installed, and noise due to scattered light in the output beams was studied and mitigated. During early 2010, monolithic suspensions were installed, which involved replacing Virgo’s test masses with new mirrors hung from fused-silica fibers. VSR3 followed this upgrade.

A measure of the sensitivity of a detector to gravitational waves is its noise power spectral density (PSD) over frequency; typical PSDs for the S6 and VSR2/3 science runs were given in [9]. Due to the improved low-frequency sensitivity of Virgo in VSR2/3 [17], the lower frequency cutoff of our analysis for V1 data was reduced to 30 Hz, compared to 40 Hz for LIGO data.

III. DATA ANALYSIS PIPELINE

Our search algorithm, which was described in detail in [3, 11], is based on matched filtering the data in each detector against a template bank of IMR waveforms, recording local maxima of signal-to-noise ratio (SNR) as *triggers*, then testing these triggers for consistency of coalescence time and mass parameters between two or more detectors via a coincidence test [18], and for their consistency with the template waveform via the χ^2 test [19]. The χ^2 test is necessary to suppress noise transients (see Section III C), which cause a much larger rate of triggers with high SNR than expected in Gaussian noise.

A. Filter templates and optimal search sensitivity

As filter templates we used the same family of waveforms as described in [3] constructed using the results of [20], which we will refer to as EOBNRv1. The parameter space covered by our templates was also unchanged, ranging from 1 to 99 M_\odot for the binary component masses m_1, m_2 , and from 25 to 100 M_\odot for the total binary mass $M = m_1 + m_2$; a search covering total mass values between 2 and 25 M_\odot was reported in [9].

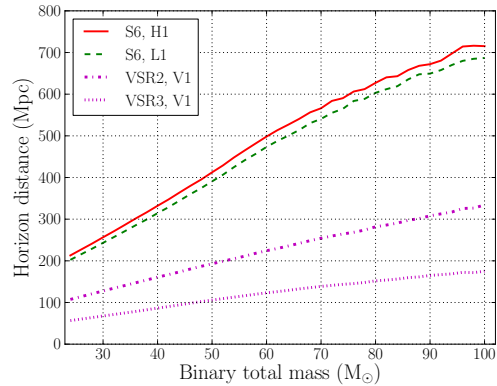


FIG. 1: Horizon distances for non-spinning equal-mass IMR signals in the LIGO and Virgo detectors, using EOBNRv2 as signal model, averaged over periods of data when the detector sensitivities were near optimal for S6 and VSR2 and -3, respectively.

The recently-implemented EOBNRv2 [12] and IMRPhenomB [13] waveforms are more accurate than their predecessors in that they are better fits to waveforms produced by numerical relativity (NR) simulations, and because the NR waveforms themselves have improved in accuracy and cover a wider range of parameter space [21, 22], [23, 24]. We discuss the relevant properties of the EOBNRv2 and IMRPhenomB waveform models in Sections V B and V C.

We investigated whether these improved waveform families could be efficiently detected by a bank of EOBNRv1 filter templates. The method used was to calculate the overlap between an EOBNRv2 or IMRPhenomB signal waveform and an EOBNRv1 template, maximizing over the parameters of the EOBNRv1 template (see [25] for the general method). For EOBNRv2 signals, over the range of mass ratio $1 \leq q \equiv m_1/m_2 \leq 6$ and total mass $25 \leq M/M_\odot \leq 100$, in the worst case the maximized overlap (effectualness) of EOBNRv1 templates was greater than 0.97. For non-spinning IMRPhenomB signals, the smallest effectualness was greater than 0.98. Thus, the use of EOBNRv1 templates did not significantly degrade the efficiency of our search, for non-spinning signals. The more recent waveform families are, however, useful in more accurately determining the sensitivity of the search to astrophysical BBH mergers.

As a simple measure of the maximum possible search sensitivity, we show in Figure 1 the horizon distances for equal-mass EOBNRv2 signals, defined as the distances at which an optimally-oriented coalescence directly overhead from a given detector would have an expected SNR of 8 for an optimal matched filter; as in [9] we average these distances over periods of data for which the detector sensitivities were optimal, or close to optimal, over each science run. We see that the maximum sensitive distance for a (20,20) M_\odot coalescence in each of the LIGO detectors was approximately 300 Mpc. The detector sensitivities varied significantly over the observation time of

this search, as detailed in [26]. Sensitive distances averaged over observation time and over source sky location and orientation are reported in Section V B.

B. Background estimate and event ranking statistic

After obtaining a list of candidate coincident events, each consisting of two or more triggers with consistent template masses and coalescence times, we estimate the significance of each event relative to background. Our background distribution is obtained by finding coincident events after applying unphysical time-shifts (greater than light travel time) to data from different detectors; we performed 100 time-shifted analyses using multiples of a (0, 5, 10) s time offset for (H1, L1, V1) data, respectively. In order to compare the coincident events to background we require a ranking statistic.

The aim of our ranking statistic is to optimize the separation of signal from background in the search. We tuned it by studying the distributions of triggers over SNR (ρ) and χ^2 for time-shifted background events, and for events resulting from simulated IMR signals added to the data (“software injections”). We found that the distribution of background triggers depended strongly on *template duration*, a trigger parameter determined by the binary component masses and by the lower frequency cutoff used in the analysis, which was taken to be 40 Hz for LIGO data and 30 Hz for Virgo. Template durations varied between approximately 0.05 s for templates with the highest total mass $100 M_\odot$, in the LIGO detectors, to several seconds for lower-mass signals. We compare signal-background separation for triggers from longer *vs.* shorter-duration templates, in a representative period of LIGO data, in Figure 2. The performance of the χ^2 test was markedly worse for templates shorter than 0.2 s in LIGO and VSR3 data, with some noise triggers in these templates having large SNR but a relatively small χ^2 value, comparable to simulated IMR signals. For signals seen in LIGO, this threshold value of 0.2 s corresponds to a total mass of approximately $45 M_\odot$ for equal-mass systems, or a total mass of approximately $90 M_\odot$ for the most asymmetric templates used in the search.

The poor performance of the χ^2 test for short templates in LIGO and VSR3 data can be attributed to the small number of template cycles over which SNR is accumulated in the templates. By contrast, the χ^2 test was found to be effective in penalizing noise artefacts in VSR2 data over the entire parameter space of the search.

We divided coincident events into two bins: one for which all participating triggers from H1 or L1 (or V1, in VSR3 data) had template durations above 0.2 s (“long duration events”) and one where at least one trigger from H1 or L1 (or V1, in VSR3) had a template duration below 0.2 s (“short duration events”).

Due to the different distributions of background triggers over SNR and χ^2 for longer-duration *vs.* shorter-duration templates, as illustrated in Figure 2, we found

that a different choice of ranking statistic was appropriate for the two bins. For all triggers participating in long duration events, and all V1 triggers in VSR2 data, we used the re-weighted SNR $\hat{\rho}$ statistic [9] defined as

$$\hat{\rho} = \begin{cases} \frac{\rho}{[(1 + (\chi_r^2)^3)/2]^{1/6}} & \text{for } \chi_r^2 > 1, \\ \rho & \text{for } \chi_r^2 \leq 1, \end{cases} \quad (1)$$

where $\chi_r^2 \equiv \chi^2/(2p - 2)$, and where we chose the number of frequency intervals p used in the evaluation of χ^2 [19] to be 10 [3]. For H1 or L1 triggers, or V1 triggers in VSR3 data, participating in short duration events we used the effective SNR statistic of [3]:

$$\rho_{\text{eff}} = \frac{\rho}{[\chi_r^2(1 + \rho^2/50)]^{1/4}}. \quad (2)$$

The detection statistic, “combined SNR” ρ_c , is then given by the quadrature sum of single-detector statistics, over the coincident triggers participating in an event.¹

We calculate the detection statistic values separately in different coincident times (times when two or more detectors are recording data, labelled by the active detectors), due to their different background event distributions and different sensitivity to astrophysical signals. The FARs of coincident events are estimated by first comparing their ρ_c values to those of time-shifted background events in the same bin by duration, and with the same event type (*i.e.* the same detectors participating in coincidence). The final detection statistic of the search, combined FAR, is determined by ranking the event’s FAR against the total distribution of background FAR values, summed over both bins in template duration and over all event types within each coincident time: see Eq. (III.7-8) of [3].

C. Data quality vetoes

The gravitational-wave strain data from the detectors contains a larger number of transient noise events (glitches) with high amplitude than would occur in colored Gaussian noise. In order to diagnose and remove these transients, each of the LIGO and Virgo observatories is equipped with a system of environmental and instrumental monitors that have a negligible sensitivity to gravitational waves but may be sensitive to glitch sources. These sensors were used to identify times when the detector output was potentially corrupted [27–30]. We grouped these times into two categories: periods with strong and well-understood couplings between non-GW

¹ Note that, as in previous searches, we applied a weak ρ -dependent cut on the χ_r^2 values, to remove triggers with very low statistic values: the effect of this cut may be seen in Figure 2 where the top left of each plot is empty.

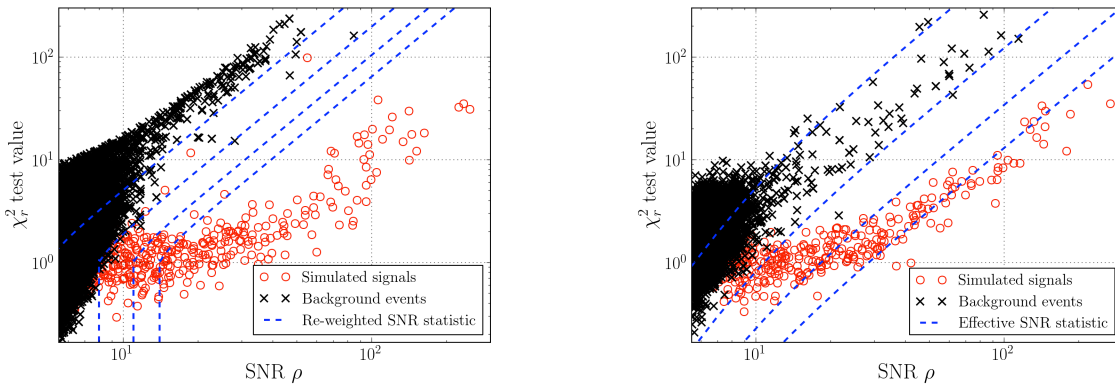


FIG. 2: Representative distributions of SNR and χ_r^2 values for simulated signal (red circle) and background (black ‘ \times ’) triggers in the LIGO detectors, with contours of the detection statistics used in the search. Note the systematically lower values of χ^2 for background events with SNR $\rho > 10$ in shorter-duration templates (right plot) compared to longer-duration (left plot). *Left*—triggers with template duration greater than 0.2s; dashed lines indicate contours of constant re-weighted SNR statistic, Eq. (1). *Right*—triggers with template duration below 0.2s; dashed lines indicate contours of constant effective SNR, Eq. (2).

transient noise sources and detector output, and periods when a statistical correlation was found although a coupling mechanism was not identified. In our primary search, both for the identification of GW candidates and the calculation of upper limits, times in both these categories, and any coincident events falling in these times, were removed (“vetoed”) from the analysis. We also performed a secondary search for possible loud candidate events, in which only times with clear coupling of non-GW transients to detector output were vetoed. The total time searched for GW candidate events, in which only the first category of vetoes were applied, was 0.53 yr.

Even after applying vetoes based on auxiliary (environmental and instrumental) sensors, significant numbers of delta-function-like glitches with large amplitude remained unvetoes in the LIGO detectors. It was found that these caused artifacts in the matched filter output over a short time surrounding the glitch: thus, 8s of time on either side of any matched filter SNR exceeding 250 was additionally vetoed. Times removed from the primary search by this veto were still examined for loud candidate events.

Approximately 0.47 yr of coincident search time remained after applying all vetoes. Additionally, approximately 10% of the data, designated *playground*, was used for tuning and data quality investigations. These data were searched for gravitational waves, but not used in calculating upper limits. After all vetoes were applied and playground time excluded, there was 0.09 yr of H1L1V1 coincident time, 0.17 yr of H1L1 time, 0.10 yr of H1V1 time, and 0.07 yr of L1V1 time, giving a total analysis time of 0.42 yr.

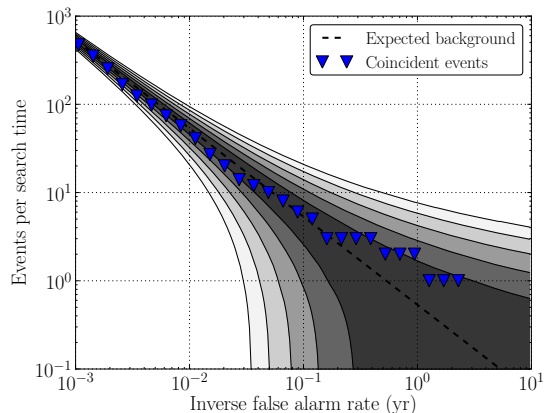


FIG. 3: Cumulative distribution of coincident events found in the search *vs.* estimated inverse false alarm rate (FAR), over the total time searched for possible GW candidates, 0.53 yr. Grey contour shading indicates the consistency at 1σ (dark) through 5σ (light) level of search coincident events with the expected background.

IV. SEARCH RESULTS

We found no significant or plausible gravitational-wave detection candidates above the noise background of the search. The cumulative distribution of coincident events found in the search *vs.* estimated inverse false alarm rate (FAR) is shown in Figure 3. The distribution is consistent with the expected background over the total time searched for GW candidates, 0.53 yr.

The most significant coincident event found in the search, with lowest estimated FAR (highest inverse FAR), was at GPS time 939789782 and had an estimated FAR of 0.41 yr^{-1} . This event, an H1V1 coincidence in H1V1 coincident time with SNR values of

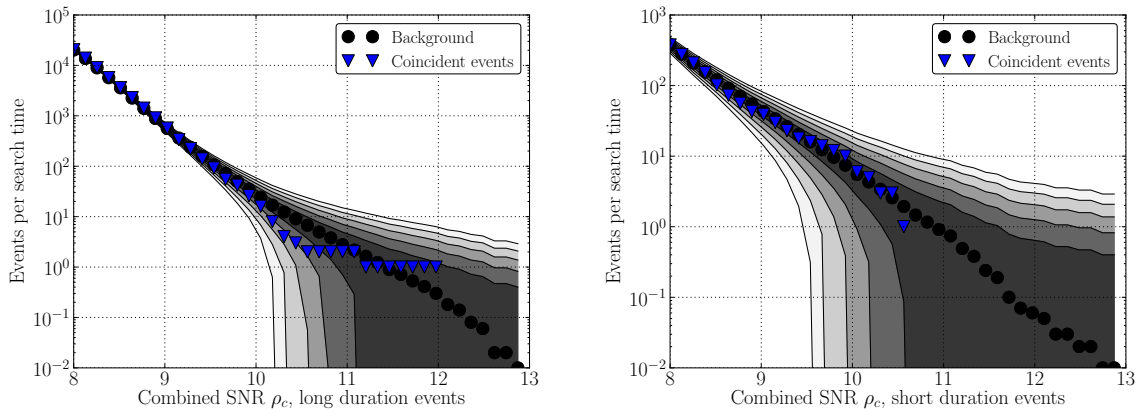


FIG. 4: Cumulative distributions of coincident events and estimated background over combined SNR statistic ρ_c , over the total time searched for possible GW candidates. Grey shaded bands indicate 1σ – 5σ consistency with the estimated background distribution. *Left*—Distribution for “long duration” events. *Right*—Distribution for “short duration” events. The two event bins and the combined SNR statistic are described in Section III B.

31 in H1 and 5.50 in V1 and a combined SNR statistic value of $\rho_c = 11.98$, occurred at a time when several short-duration, non-Gaussian transient excess power events were visible, over a period of several seconds, in time-frequency maps of the GW strain channel in H1. The high trigger SNR in H1 was caused by the first of these transients; however the behavior of the strain and SNR time series over the following few seconds is strongly inconsistent with a high-mass binary coalescence signal. The χ^2 test value in H1 was high (approximately 190), but not sufficiently high to rule out the trigger as a candidate.

The frequency spectrum of the noise transients in H1 indicates their probable origin as stray light scattered into the interferometer beam. The appearance of the event in V1 was consistent with both a quiet GW signal and with random noise. The event time was not vetoed in the search, as none of the instrumental or environmental channels at H1 which we found to be significantly correlated with noise transients in the GW channel showed a malfunction at the event time.

The second loudest event was at GPS 963363786 with an estimated FAR of 1.0 yr^{-1} . It was an H1L1 coincidence in H1L1 time with SNRs of 13 in H1 and 70 in L1 and a combined SNR statistic value of $\rho_c = 10.48$. This time was subject to a veto in H1, due to a problem in a high-voltage power supply near the output photodiodes (affecting some weeks of data) which caused bursts of broad-band non-Gaussian noise. However, since this excess noise was not sufficiently severe to preclude detection, the time was still searched for possible high-SNR candidate events, as described in Section III C. The trigger in L1 was caused by a high amplitude non-Gaussian transient of very short duration, part of a population of sporadic glitches for which no effective veto could be found. This event also failed a detailed followup, as time-frequency maps of excess power, and the time series of

SNR and χ^2 in H1, were inconsistent with an IMR signal.

The next few most significant events had estimated FARs of a few per year and were thus entirely consistent with background.

We show the ρ_c distributions of coincident events and time-shifted background events, for the total time searched for possible GW candidates, in Figure 4, separating the long- and short-duration events since ρ_c is a different function of ρ and χ^2 in each. The ρ_c values of all the loudest search events were less than 12 (for comparison, a BBH coalescence signal with an SNR of 8 in each of two detectors would give approximately $\rho_c \simeq 11.3$). Thus, the data quality veto procedure, in combination with the signal-based χ^2 test, were sufficient to remove or suppress loud detector artefacts to a level where the sensitivity of our search is not greatly impaired.

V. UPPER LIMITS ON BBH COALESCENCE RATES

Given the null result of our search for BBH coalescence signals, we wish to set observational limits on the astrophysical rates of such signals, over regions of parameter space where our search has non-negligible sensitivity. As discussed in [3], the distance reach of this high-mass search is such that the source population can be treated as approximately homogeneous over spatial volume; thus we aim to set limits on the rate density of coalescences, in units of $\text{Mpc}^{-3}\text{ yr}^{-1}$.

A. Upper limit calculation procedure

Our upper limit calculation is similar to that performed in [9]: it is based on the loudest event statistic [31] applied as described in Section V of [3] with minor im-

improvements in implementation. We divide the data into 9 periods of approximately 6 weeks each; in 4 of these only H1L1 coincident time was recorded, whereas in the remaining 5 we had four types of coincident time (H1L1, H1V1, L1V1 and H1L1V1).

In each of the resulting 24 analysis times, we estimate the volume to which the search is sensitive by reanalyzing the data with the addition of a large number of simulated signals (“software injections”) in order to model the source population. Our ability to detect a signal depends upon the parameters of the source, including the component masses and spins (magnitudes and directions), the distance to the binary, its sky location, and its orientation with respect to the detectors. Numerous signals with randomly chosen parameter values were therefore injected into the data.

To compute the sensitive volume over a given range of binary masses (“mass bin”), we perform a Monte Carlo integration over the other parameters to obtain the efficiency of the search—determined by the fraction of simulated signals found louder than the loudest observed coincident event in each analysis time—as a function of distance. Integrating the efficiency over distance then gives the sensitive volume for that analysis time, and an associated sensitive distance.

We then estimate the likelihood parameter Λ of signal *vs.* background at the combined FAR value of the loudest observed event in each analysis time, for each mass bin, as described in [3, 31]. Using these Λ values and the estimated sensitive volumes we find the probability of the measured loudest FAR value as a function of the astrophysical merger rate, *i.e.* the likelihood of the data given the model, in each analysis time and for each mass bin. Given a prior probability distribution over the rate, in each mass bin, we then multiply by the likelihoods of the loudest events from all the analysis times to form a posterior over rate: see [3] (Section V and Erratum) for relevant formulae.

The likelihood function for each analysis time depends on the sensitive volume \times time searched; however, the sensitive volumes have statistical uncertainties due to the finite number of injections performed in each mass bin, and systematic uncertainties in the amplitude calibration for each detector. As detailed in [9], we take an overall 42% uncertainty in volume due to calibration errors. We marginalize over statistical uncertainties for each analysis time separately, but since systematic calibration errors may be significantly correlated between analysis times we perform this marginalization [32] once after combining the likelihoods from all analysis times. We then find the 90% confidence upper limit based on the marginalized posterior distributions over rate.

We also calculated an average sensitive distance in each mass bin, defined as the radius of a sphere such that the sphere’s volume, multiplied by the total search time, equals the total sensitive volume \times time over all analysis times.

Since the injected waveforms are phenomenological

models, our upper limits will also be systematically affected to the extent that the true IMR waveforms differ from these models. These uncertainties are difficult to quantify over the search as a whole and we will not attempt to incorporate them into our quoted limits. A comparison of EOBNRv2 waveforms against numerical relativity simulations for mass ratios $q = 1, 4, 6$ shows possible SNR biases of at most a few percent within the total mass range $25 \leq M/M_\odot \leq 100$.

The rate priors that we use for non-spinning EOBNRv2 signals in the S6-VSR2/3 search are derived from the results of the S5 high-mass BBH search [3]. The original results from this search were affected by an incorrect treatment of marginalization over errors in the sensitive volume and flaws in the numerical procedure used to estimate the Λ values, resulting overall in an over-conservative set of 90% rate upper limits. These problems were recently addressed, leading to revised upper limits from S5 data ([3], Erratum); the resulting revised posteriors over coalescence rate were used as priors for our main upper limit calculation. Revised rate upper limits from S5 data alone are also included in Table I. Note that, as priors *for the S5 calculation*, uniform probability distributions over rate were taken; this uniform prior is a conservative choice for setting upper limits.

B. Rate limits from EOBNRv2 injections

In order to evaluate the search sensitivity to non-spinning IMR signals over a wide parameter space, and to allow a comparison to previous search results, we used an implementation of the recently developed EOBNRv2 waveform family [12] as simulated signals.

The EOBNRv2 waveform family was designed using results from [33–36]. The inspiral waveforms in the EOBNRv2 model are improved over EOBNRv1 by calibrating two adjustable parameters against five highly accurate NR simulations of mass ratios $q = 1, 2, 3, 4$ and 6, generated by the pseudospectral code SpEC [23, 24]. These two parameters are the pseudo-4PN and 5PN coefficients a_5 and a_6 entering the EOB radial potential (see, *e.g.*, Eq. (II7a) in Ref. [3] and related discussion.) EOBNRv2 also improves over EOBNRv1 by including all known post-Newtonian (PN) corrections in the amplitude, by using a more accurate estimate of the radiated energy flux, by dropping the assumption of quasi-circular orbits, by improving the matching of the inspiral-plunge waveform to the ringdown modes, and by improving the extrapolation to large mass ratios. The differences between these EOBNRv2 and NR waveforms are comparable with numerical errors in the NR simulations.

EOBNRv2 injections were distributed to “over-cover” the parameter range of the search, in order to ensure complete coverage of the mass bins used in [3]. The injections were distributed approximately uniformly over the component masses m_1 and m_2 , within the ranges $1 M_\odot \leq m_i \leq 99 M_\odot$ and $20 M_\odot \leq M \leq 109 M_\odot$.

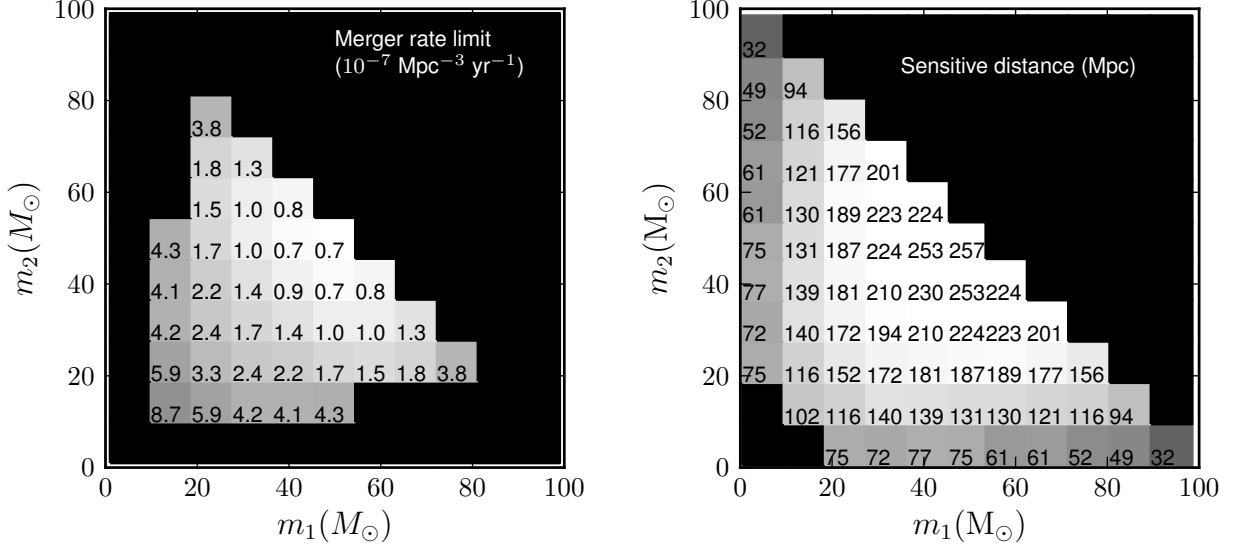


FIG. 5: *Left*—Upper limits (90% confidence) on BBH coalescence rates in units of $10^{-7} \text{ Mpc}^{-3} \text{ yr}^{-1}$ as a function of binary component masses, evaluated using EOBNRv2 waveforms. *Right*—Average sensitive distance for this search to binary systems described by EOBNRv2 signal waveforms, in Mpc.

TABLE I: Search sensitive distances and coalescence rate upper limits, quoted over $9 M_\odot$ -wide component mass bins labelled by their central values. We also quote the chirp mass \mathcal{M} at the centre of each bin. The sensitive distance in Mpc (averaged over the observation time and over source sky location and orientation) is given for EOBNR waveforms in S5 data rescaled for consistency with NR results [3], and for EOBNRv2, IMRPhenomB non-spinning (“PhenomB nonspin”) and IMRPhenomB spinning (“PhenomB spin”) waveforms in the S6-VSR2/3 data. The last two columns report 90%-confidence rate upper limits in units of $10^{-7} \text{ Mpc}^{-3} \text{ yr}^{-1}$, for bins with component mass ratios $1 \leq m_1/m_2 \leq 4$, for S5 data (revised relative to [3]) and the cumulative upper limits over S5 and S6-VSR2/3 data, as presented in this work.

Waveforms Search data			EOBNR S5	EOBNR S6-VSR2/3	PhenomB nonspin S6-VSR2/3	PhenomB spin S6-VSR2/3	EOBNR S5	EOBNR S5 + S6-VSR2/3
m_1 (M_\odot)	m_2 (M_\odot)	\mathcal{M} (M_\odot)	Distance (Mpc)	Distance (Mpc)	Distance (Mpc)	Distance (Mpc)	Upper Limit ($10^{-7} \text{ Mpc}^{-3} \text{ yr}^{-1}$)	Upper Limit ($10^{-7} \text{ Mpc}^{-3} \text{ yr}^{-1}$)
14	14	13	81	102	105	106	18	8.7
23	14	16	95	116	126	126	12	5.9
32	14	18	102	140	132	135	8.8	4.2
41	14	21	107	139	141	145	7.8	4.1
50	14	22	107	131	137	149	8.2	4.3
23	23	20	116	152	148	149	7.4	3.3
32	23	24	133	172	172	179	4.9	2.4
41	23	27	143	181	178	183	4.3	2.2
50	23	29	145	187	188	198	3.4	1.7
59	23	32	143	189	188	192	3.2	1.5
68	23	34	140	177	180	191	3.7	1.8
77	23	36	119	156	176	170	5.6	3.8
32	32	28	148	194	190	197	3.4	1.7
41	32	32	164	210	219	220	2.5	1.4
50	32	35	177	224	221	214	1.9	1.0
59	32	38	174	223	221	214	2.0	1.0
68	32	40	162	201	199	210	2.4	1.3
41	41	36	183	230	222	224	1.6	0.9
50	41	39	191	253	253	258	1.4	0.7
59	41	43	194	224	239	236	1.4	0.8
50	50	44	192	257	218	217	1.4	0.7

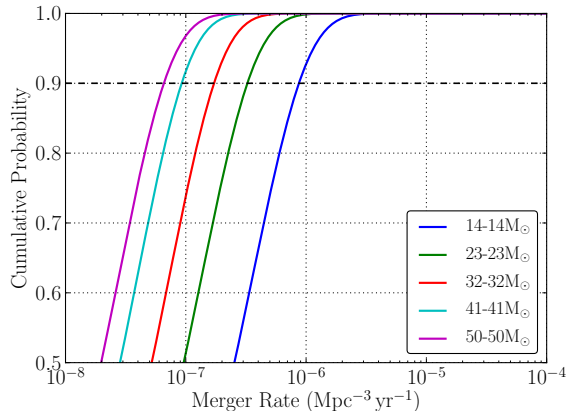


FIG. 6: Cumulative posterior probabilities over astrophysical merger rate, for the bins shown in Figure 5 with central values $m_1 = m_2 = 50, 41, 32, 23, 14 M_\odot$ (left to right). We show the probability level corresponding to the 90% confidence rate limit (dashed horizontal line). These posteriors were evaluated for signals described by the EOBNRv2 waveform family in S6 data using S5 search results as prior information.

The resulting 90% confidence upper limits on non-spinning coalescence rates are displayed in Figure 5, left plot, and in Table I. These upper limits supersede those reported in [3]. As explained in the previous section, we used revised priors over rate from the S5 analysis. These were obtained using (non-spinning) EOBNRv1 simulated signals, and a smaller number of IMRPhenomA simulations. As described in [3] their distances were appropriately adjusted to account for the amplitude bias of the older waveform families, by comparison with current NR simulations of BBH merger. Due to the restricted range of parameters of NR simulations available at the time of the previous analysis, we quote limits on astrophysical rates only for bins within the range of mass ratio $1 \leq q \leq 4$. For binaries with both component masses lying between 19 and $28 M_\odot$ we find a 90% limit of 3.3×10^{-7} mergers $\text{Mpc}^{-3}\text{yr}^{-1}$.

The averaged sensitive distance to simulated EOBNRv2 waveforms over the S6-VSR2/3 observation time, for the entire parameter space of the search, is displayed in Figure 5, right plot.

To illustrate our statistical upper limit method we display the cumulative posterior probabilities over coalescence rate, for a selection of the mass bins of Figure 5 covering the equal-mass line $m_1 = m_2$, in Figure 6. This figure shows the dependence of the quoted upper limit on the confidence level; we choose to use a 90% confidence limit as indicated by the dashed line.

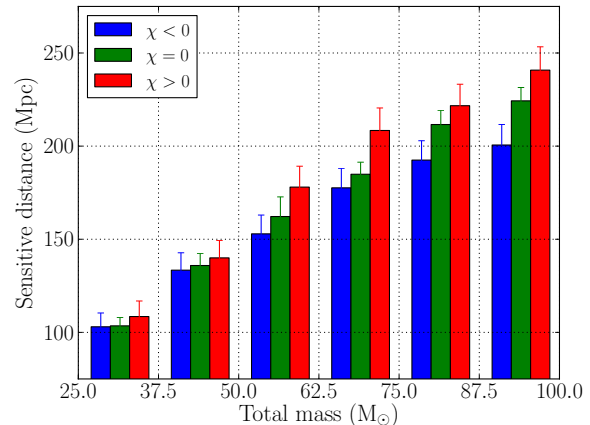


FIG. 7: Dependence on aligned spin and total mass of the averaged sensitive distance of our search to phenomenological inspiral-merger-ringdown waveforms. For each of 6 bins in total mass M , we show the sensitivity for IMRPhenomB signals with negative aligned spin parameter χ (left), non-spinning signals (centre) and signals with positive aligned spin parameter (right). The simulated signal parameters were restricted to mass ratios $1 \leq q < 4$ and aligned spins $-0.85 \leq \chi \leq 0.85$.

C. Sensitivity to non-spinning and spinning IMRPhenomB injections

The spins of the component black holes are known to have a potentially large effect on the emitted IMR waveform (e.g. [37, 38]), affecting the phase evolution and, in the case of spins significantly out of alignment with the orbital angular momentum, producing amplitude modulations due to precession [39]. X-ray observations of the spins of accreting black holes in binary systems, while technically challenging, indicate a fairly uniform distribution over the entire range $0 \leq a \equiv S/m^2 \leq 1$ [40–46]. Note that such measurements apply to black holes in X-ray binaries, which may not be representative of spins in BBH systems.

Indications that spin-orbit misalignment in field binaries may be small come from observations of the microquasar XTE J1550-564 [47], and from population synthesis models [48]. For dynamically formed binaries, however, the component spins may be largely independent of each other and of the orbital parameters.

In any case it is desirable to perform injections using spinning BBH coalescence waveforms, in order to estimate how far our search was sensitive to such signals. Knowledge of spinning BBH coalescence waveforms is, however, currently limited to a relatively small number of numerical relativity simulations (see [13] and references therein), most having spin magnitudes significantly below unity, and only a few including non-aligned spins. Only very recently have simulations for near-extreme spins [49] been performed. Thus, as a first step towards quantifying the sensitivity of the search to spin-

ning waveforms over a broad parameter space, we use the IMRPhenomB waveform family [13] which models IMR signals from BBH with aligned/anti-aligned spins. This waveform family is parametrized by the total mass $M \equiv m_1 + m_2$, the mass ratio $q \equiv m_1/m_2$ and a single aligned spin parameter χ ,² defined for spins S_i parallel to the orbital angular momentum as

$$\chi \equiv \frac{m_1}{M} \chi_1 + \frac{m_2}{M} \chi_2, \quad (3)$$

where $\chi_i \equiv \mathbf{S}_i \cdot \hat{\mathbf{L}}/m_i^2$ is the dimensionless spin of black hole i projected onto the orbital angular momentum \mathbf{L} . These waveforms are calibrated against numerical-relativity simulations in the parameter range $1 \leq q \leq 4$ and $-0.85 \leq \chi \leq 0.85$, and, for the inspiral part, to the calculated evolution in the extreme-mass-ratio (test mass) limit. The waveform family is constructed in the frequency domain and then converted to the time domain via an inverse discrete Fourier transform.

As simulated signals we used two sets of IMRPhenomB injections, a non-spinning set and a spinning set. Both were uniformly distributed in total mass between 25 and 100 M_\odot , and uniformly distributed in $q/(q+1) \equiv m_1/M$ for a given M , between the limits $1 \leq q < 4$. In addition, the spinning injections were assigned aligned spin components χ_i uniformly distributed between -0.85 and 0.85.

To illustrate the effect of aligned spin on the search sensitivity, we plot in Figure 7 the average sensitive distance over the S6-VSR2/3 observation time, in bins of total mass M , for both non-spinning simulated signals and for injections with $\chi < 0$ and $\chi > 0$ respectively.

Component spin is expected to have several effects on our search, compared to its performance for non-spinning systems. First, the amplitude of the expected signal from a coalescence at a given distance may depend on spin: see for instance Figure 3 of [13], where the horizon distance for IMRPhenomB signals with optimally fitting templates, with Initial LIGO noise spectra, was found to increase steeply with increasing positive χ . Second, the EOBNR templates used in our search may have reduced overlap with the simulated spinning signals, leading to a loss of sensitivity. Third, the signal-based χ^2 test values are expected to be higher than if exactly matched spinning templates were used, due to “un-matched” excess power in the signals; this would further reduce the search sensitivity. Given the complexity of the search pipeline, it is not clear which effect would dominate. Figure 7 indicates higher sensitivity to positive- χ signals even with the current non-spinning templates, but also shows that the search is significantly less sensitive to negative- χ signals at higher values of total mass M .

² This parameter is not to be confused with the χ^2 test mentioned earlier in Section III.

D. Waveforms including higher spherical harmonic modes

In the filter templates and in all injections used in this search, we consider only the dominant mode of GW emission from coalescing binaries, the $(l, m) = (2, 2)$ mode. In general, higher-order modes are important in BBH with asymmetric masses and significant component spins. Omitting these modes in templates will neglect their contributions to the SNR [50, 51], and may also lead to a worse (higher) value of the χ^2 test, tending to reduce the sensitivity of the search. However, such effects will depend strongly on the mass ratio and on extrinsic (angular) parameters, and it is beyond the scope of this analysis to investigate them in detail.

In [12] the mismatch between NR waveforms containing the strongest 7 modes observed with a binary inclination angle of $\pi/3$, and EOBNRv2 templates containing only the $(l, m) = (2, 2)$ mode, was calculated using the Advanced LIGO zero-detuning high-power PSD [52]. This mismatch took values up to 10% for BBHs with mass ratio $q = 1-6$ and total mass $M < 100M_\odot$. Adding non-dominant modes to the EOBNRv2 waveforms reduced the mismatch to below 1% (for the same inclination angle and a template containing 5 modes).

E. Astrophysical implications

There is no commonly accepted astrophysical rate estimate for high-mass CBCs, owing to the many possible formation scenarios and the considerable uncertainties affecting them. In [5, 53] a rate of $3.6_{-2.6}^{+5.0} \times 10^{-7} \text{ Mpc}^{-3} \text{ yr}^{-1}$ for IMR signals from binaries with chirp mass comparable to $15 M_\odot$ was estimated based on two observed tight binaries believed to consist of a massive stellar BH and a Wolf-Rayet star. Our 90% upper rate limit for the bin with component masses $19 < m_1/M_\odot < 28$, $10 < m_2/M_\odot < 19$, for which the chirp mass ranges between 12 and 20 M_\odot , is $5.9 \times 10^{-7} \text{ mergers Mpc}^{-3} \text{ yr}^{-1}$. Thus, current searches are close to the sensitivity necessary to put nontrivial constraints on astrophysical scenarios of BBH formation and evolution. However, we remind the reader that systems with near-extremal ($S_i/m_i^2 > 0.85$) or significantly non-aligned spins, or for which higher signal harmonics make a considerable contribution to the waveform seen at the detectors, were not included in our sensitivity studies.

VI. DISCUSSION

The present search is an advance over that reported in [3] in three main respects: the improved sensitivity of the LIGO and Virgo detectors over previous science runs; improved understanding of the search background by identifying the duration of the IMR templates as the dominant

parameter controlling their output in non-Gaussian detector data; and the use of updated, more accurate signal models to assess search sensitivity, including models describing component spins aligned to the orbital angular momentum.

There are, however, many issues that remain to be addressed in order for future data from advanced detectors [14, 54] to be best exploited in searching for high-mass CBC. Among these, the metric currently used for template bank placement and for testing mass coincidence between detectors is based on the inspiral portion of CBC waveforms only. The search may be improved by using a more accurate metric for IMR waveforms, and more radically by also including spin-aligned IMR templates as matched filters, which may significantly increase the sensitivity to spinning BBH.

Separating signal from non-Gaussian noise events in short filter templates, where our signal-based χ^2 tests are not effective, remains a difficult problem. Improved methods, including the use of amplitude consistency tests between different detectors and multivariate classifiers, are currently being investigated.

Advanced detectors coming on line in the coming years will improve the sensitivity to GW relative to the first generation by a factor 10 over a broad frequency range, and will achieve good sensitivity down to a low-frequency limit of ~ 10 Hz. The volume of space over which future searches will be sensitive to IMR signals is therefore expected to increase by a factor 10^3 or more depending on the binary masses. We thus expect to extract significant information on BBH source populations over the parameter space of future searches.

Acknowledgments

The authors gratefully acknowledge the support of the United States National Science Foundation for the con-

struction and operation of the LIGO Laboratory, the Science and Technology Facilities Council of the United Kingdom, the Max-Planck-Society, and the State of Niedersachsen/Germany for support of the construction and operation of the GEO600 detector, and the Italian Istituto Nazionale di Fisica Nucleare and the French Centre National de la Recherche Scientifique for the construction and operation of the Virgo detector. The authors also gratefully acknowledge the support of the research by these agencies and by the Australian Research Council, the International Science Linkages program of the Commonwealth of Australia, the Council of Scientific and Industrial Research of India, the Istituto Nazionale di Fisica Nucleare of Italy, the Spanish Ministerio de Economía y Competitividad, the Conselleria d'Economia Hisenda i Innovació of the Govern de les Illes Balears, the Foundation for Fundamental Research on Matter supported by the Netherlands Organisation for Scientific Research, the Polish Ministry of Science and Higher Education, the FOCUS Programme of Foundation for Polish Science, the Royal Society, the Scottish Funding Council, the Scottish Universities Physics Alliance, The National Aeronautics and Space Administration, the National Research Foundation of Korea, Industry Canada and the Province of Ontario through the Ministry of Economic Development and Innovation, the National Science and Engineering Research Council Canada, the Carnegie Trust, the Leverhulme Trust, the David and Lucile Packard Foundation, the Research Corporation, and the Alfred P. Sloan Foundation.

-
- [1] B. Abbott et al. (LIGO Scientific Collaboration), *Rep. Prog. Phys.* **72**, 076901 (2009).
 - [2] T. Accadia et al. (Virgo Collaboration), *JINST* **7**, P03012 (2012).
 - [3] J. Abadie et al. (LIGO Scientific Collaboration and Virgo Collaboration), *Phys. Rev. D* **83**, 122005 (2011), erratum: *ibid.* **86**, 069903(E) (2012), arXiv:1102.3781.
 - [4] J. Abadie et al. (LIGO Scientific Collaboration and Virgo Collaboration), *Class. Quant. Grav.* **27**, 173001 (2010).
 - [5] T. Bulik, K. Belczynski, and A. Prestwich, *Astrophys. J.* **730**, 140 (2011), arXiv:0803.3516.
 - [6] S. W. Davis, R. Narayan, Y. Zhu, D. Barret, S. A. Farrell, O. Godet, M. Servillat, and N. A. Webb, *Astrophys. J.* **734**, 111 (2011), arXiv:1104.2614.
 - [7] K. Belczynski, M. Dominik, T. Bulik, R. O'Shaughnessy, C. Fryer, and D. E. Holz, *Astrophys. J.* **715**, L138 (2010), arXiv:1004.0386.
 - [8] M. Dominik, K. Belczynski, C. Fryer, D. Holz, E. Berti, T. Bulik, I. Mandel, and R. O'Shaughnessy, *Astrophys. J.* **759**, 52 (2012), arXiv:1202.4901.
 - [9] J. Abadie et al. (LIGO Scientific Collaboration and Virgo Collaboration), *Phys. Rev. D* **85**, 082002 (2012), arXiv:1111.7314.
 - [10] J. Abadie et al. (LIGO Scientific Collaboration and Virgo Collaboration), *Phys. Rev. D* **85**, 102004 (2012), arXiv:1201.5999.
 - [11] S. Babak et al., *Phys. Rev. D*, to be published (2013), arXiv:1208.3491.
 - [12] Y. Pan, A. Buonanno, M. Boyle, L. T. Buchman, L. E. Kidder, H. P. Pfeiffer, and M. A. Scheel, *Phys. Rev. D* **84**, 124052 (2011), arXiv:1106.1021.
 - [13] P. Ajith et al., *Phys. Rev. Lett.* **106**, 241101 (2011), arXiv:0909.2867.
 - [14] G. M. Harry and the LIGO Scientific Collaboration, *Class. Quant. Grav* **27**, 084006 (2010).
 - [15] R. Adhikari, P. Fritschel, and S. Waldman, *Tech.*

- Rep. LIGO-T060156-v1, LIGO Project (2006), URL <https://dcc.ligo.org/cgi-bin/DocDB/ShowDocument?docid=7384>.
- [16] T. Accadia et al. (Virgo Collaboration), *Class. Quant. Grav.* **28**, 025005 (2011), arXiv:1009.5190.
- [17] T. Accadia et al. (Virgo Collaboration), *J. Low Freq. Noise Vib. Active Control* **30**, 63 (2011).
- [18] C. A. K. Robinson, B. S. Sathyaprakash, and A. S. Sengupta, *Phys. Rev. D* **78**, 062002 (2008).
- [19] B. Allen, *Phys. Rev. D* **71**, 062001 (2005).
- [20] A. Buonanno et al., *Phys. Rev. D* **76**, 104049 (2007), arXiv:0706.3732.
- [21] M. Hannam et al., *Phys. Rev. D* **77**, 044020 (2008), arXiv:0706.1305.
- [22] M. Hannam, S. Husa, F. Ohme, D. Muller, and B. Bruegmann, *Phys. Rev.* **D82**, 124008 (2010), arXiv:1007.4789.
- [23] L. T. Buchman, H. P. Pfeiffer, M. A. Scheel, and B. Szilágyi, *Phys. Rev. D* **86**, 084033 (2012), arXiv:1206.3015.
- [24] <http://www.black-holes.org/SpEC.html>.
- [25] T. Damour, B. R. Iyer, and B. S. Sathyaprakash, *Phys. Rev. D* **57**, 885 (1998).
- [26] J. Abadie et al. (LIGO Scientific Collaboration and Virgo Collaboration) (2012), 1203.2674.
- [27] J. Slutsky et al., *Class. Quant. Grav.* **27**, 165023 (2010), arXiv:1004.0998.
- [28] N. Christensen (for the LIGO Scientific Collaboration and the Virgo Collaboration), *Class. Quant. Grav.* **27**, 194010 (2010).
- [29] F. Robinet (for the LIGO Scientific Collaboration and the Virgo Collaboration), *Class. Quant. Grav.* **27**, 194012 (2010).
- [30] D. Macleod et al., *Class. Quant. Grav.* **29**, 055006 (2012), 1108.0312.
- [31] R. Biswas, P. R. Brady, J. D. E. Creighton, and S. Fairhurst, *Class. Quant. Grav.* **26**, 175009 (2009).
- [32] P. R. Brady and S. Fairhurst, *Class. Quant. Grav.* **25**, 105002 (2008).
- [33] T. Damour, B. R. Iyer, and A. Nagar, *Phys. Rev. D* **79**, 064004 (2009).
- [34] T. Damour and A. Nagar, *Phys. Rev. D* **79**, 081503 (2009).
- [35] Y. Pan, A. Buonanno, R. Fujita, E. Racine, and H. Tagoshi, *Phys.Rev.* **D83**, 064003 (2011), arXiv:1006.0431.
- [36] E. Barausse, A. Buonanno, S. A. Hughes, G. Khanna, S. O’Sullivan, et al., *Phys. Rev. D* **85**, 024046 (2012), arXiv:1110.3081.
- [37] M. Campanelli, C. O. Lousto, Y. Zlochower, B. Krishnan, and D. Merritt, *Phys. Rev. D* **75**, 064030 (2007).
- [38] M. Campanelli, C. Lousto, and Y. Zlochower, *Phys.Rev.* **D74**, 041501 (2006).
- [39] T. A. Apostolatos, C. Cutler, G. J. Sussman, and K. S. Thorne, *Phys. Rev. D* **49**, 6274 (1994).
- [40] J. Miller, C. Reynolds, A. Fabian, G. Miniutti, and L. Gallo, *Astrophys. J.* **697**, 900 (2009), arXiv:0902.2840.
- [41] R. Shafee, J. E. McClintock, R. Narayan, S. W. Davis, L.-X. Li, and R. A. Remillard, *Astrophys. J.* **636**, L113 (2006).
- [42] J. E. McClintock et al., *Astrophys. J.* **652**, 518 (2006).
- [43] J. Liu, J. E. McClintock, R. Narayan, S. W. Davis, and J. A. Orosz, *Astrophys. J.* **719**, L109 (2010).
- [44] L. Gou et al., *Astrophys. J.* **701**, 1076 (2009), arXiv:0901.0920.
- [45] S. W. Davis, C. Done, and O. M. Blaes, *Astrophys. J.* **647**, 525 (2006).
- [46] L.-X. Li, E. R. Zimmerman, R. Narayan, and J. E. McClintock, *Astrophys. J.s* **157**, 335 (2005).
- [47] J. F. Steiner and J. E. McClintock, *Astrophys. J.* **745**, 136 (2012), arXiv:1110.6849.
- [48] T. Fragos, M. Tremmel, E. Rantsiou, and K. Belczynski, *Astrophys. J.* **719**, L79 (2010), arXiv:1001.1107.
- [49] G. Lovelace, M. Boyle, M. A. Scheel, and B. Szilágyi, *Class. Quant. Grav.* **29**, 045003 (2012), arXiv:1110.2229.
- [50] C. Van Den Broeck and A. S. Sengupta, *Class. Quant. Grav.* **24**, 155 (2007).
- [51] D. McKechn, Ph.D. thesis, Cardiff University (2011), arXiv:1102.1749.
- [52] D. Shoemaker (LIGO Scientific Collaboration), *Advanced LIGO anticipated sensitivity curves* (2010), LIGO Document T0900288-v3, URL <https://dcc.ligo.org/cgi-bin/DocDB/ShowDocument?docid=2974>.
- [53] K. Belczynski, T. Bulik, M. Dominik, and A. Prestwich (2011), arXiv:1106.0397.
- [54] T. Accadia et al., in *Twelfth Marcel Grossmann Meeting on General Relativity* (World Scientific, Singapore, 2012), p. 1738.